Inorg. Chem. **2007**, *46*, 1196–1204

Diastereoselective Oxidative Addition of Dihydrogen to IrI(CO)((*R*)-BINAP) and [Ir(CO)$_2$((*R*)-BINAP)][SbF$_6$]

Abdurrahman Ç. Atesin,[†] Simon B. Duckett,[‡] Christine Flaschenriem,[†] William W. Brennessel,[†] and Richard Eisenberg*,[†]

Department of Chemistry, University of Rochester, Rochester, New York 14627, and Department of Chemistry, University of York, York YO10 5DD, U.K.

Received August 4, 2006

Two chiral iridium(I) (*R*)-BINAP complexes, IrI(CO)((*R*)-BINAP) (**1**) and [Ir(CO)$_2$((*R*)-BINAP)][SbF$_6$] (**2**), have been synthesized and characterized, and their reactivity with dihydrogen has been studied. Complex **1** is formed on the addition of (*R*)-BINAP to [Bu$_4$N][IrI$_2$(CO)$_2$] in toluene, and **2** is generated by the addition of AgSbF$_6$ to a solution of **1** in dichloromethane under CO. A structure determination of complex **2** confirms a square planar coordination geometry, while that of **1** reveals a significant tetrahedral distortion from the expected planar coordination. Additionally, the structure of **1** shows a disorder between iodide and CO ligands. The reaction of **1** with H$_2$ proceeds under kinetic control and shows a high degree of kinetic and thermodynamic selectivity; the kinetic product is formed by H$_2$ addition across the P–Ir–CO axis of IrI(CO)((*R*)-BINAP) and yields two diastereomers which then convert over time to two more stable diastereomers which correspond to oxidative addition across the P–Ir–I axis. The kinetically favored diastereomers are formed in an initial ratio of 8.6:1, corresponding to a $\Delta\Delta G^*$ of 1.27 kcal/mol. The reaction of H$_2$ with the C_2-symmetric complex **2** also leads to the formation of two diastereomers, with one favored over the other kinetically by a 9.9:1 ratio on extrapolation to $t = 0$. When these reactions are followed using parahydrogen NMR methods, only one of the initially formed diastereomers in each case is found to exhibit substantial parahydrogen-induced polarization in the hydride resonances at room temperature.

Introduction

The activation of dihydrogen plays an important role in transition metal catalyzed reactions such as homogeneous hydrogenation and hydroformylation.[1−8] For d^8 Rh(I) and Ir(I) catalysts and model systems, the activation of H$_2$ proceeds by concerted oxidative addition to yield metal dihydride products with the hydride ligands in mutually cis positions. Previous work using IrX(CO)(dppe) (X = Cl, Br, I; dppe = bis(diphenylphosphino)ethane) has shown that the reaction proceeds under kinetic control, as shown in Scheme 1, leading to a kinetic dihydride product with >99% selectivity followed by isomerization to the thermodynamic dihydride in >90% yield.[9] (This isomerization involves at least two paths, one being a simple reductive elimination/oxidative re-addition sequence and the other being a bimolecular dihydride transfer[10].) The basis of the stereoselectivity was rationalized by the preferential addition to the Ir(I) complex of H$_2$ with its molecular axis parallel to the P−Ir−CO axis of the complex (see Scheme 1) relative to addition with H$_2$ parallel to the P−Ir−X axis that would lead to the thermodynamic isomer. This preference is based on electronic factors, most notably the ability of CO to stabilize the "Ir(H$_2$) trigonal bipyramidal" transition state of the H$_2$

* To whom correspondence should be addressed. E-mail: eisenberg@chem.rochester.edu.
[†] University of Rochester.
[‡] University of York.

(1) Heinekey, D. M.; Oldham, J. W. J. *Chem. Rev.* **1993**, *93*, 913−926.
(2) Collman, J. P.; Hegedus, L. S.; Norton, J. R.; Finke, R. G. *Principles and Applications of Organotransition Metal Chemistry*; University Science Books: Mill Valley, CA, 1987.
(3) Jessop, P. G.; Morris, R. H. *Coord. Chem. Rev.* **1992**, *121*, 155−284.
(4) Parshall, G. W.; Ittel, S. D. *Homogeneous Catalysis. The Applications and Chemistry of Catalysis by Soluble Transition Metal Complexes*, 2nd ed.; John Wiley and Sons, Inc.: New York, 1992.
(5) Cotton, F. A.; Wilkinson, G. *Advanced Inorganic Chemistry*, 5th ed.; John Wiley and Sons, Inc.: New York, 1988.
(6) Ungvary, F. *Coord. Chem. Rev.* **2003**, *241*, 295−312.
(7) Chaloner, P. A.; Esteruelas, M. A.; Joo, F.; Oro, L. A. *Homogeneous Hydrogenation*; Kluwer Academic Publishers: Dordrecht, The Netherlands, 1994.
(8) Knowles, W. S. *Acc. Chem. Res.* **1983**, *16*, 106−112.
(9) Johnson, C. E.; Eisenberg, R. *J. Am. Chem. Soc.* **1985**, *107*, 3148−3160.
(10) Kunin, A. J.; Johnson, C. E.; Maguire, J. A.; Jones, W. D.; Eisenberg, R. *J. Am. Chem. Soc.* **1987**, *109*, 2963−2968.

10.1021/ic061471a CCC: $37.00
Published on Web 01/24/2007

Scheme 1

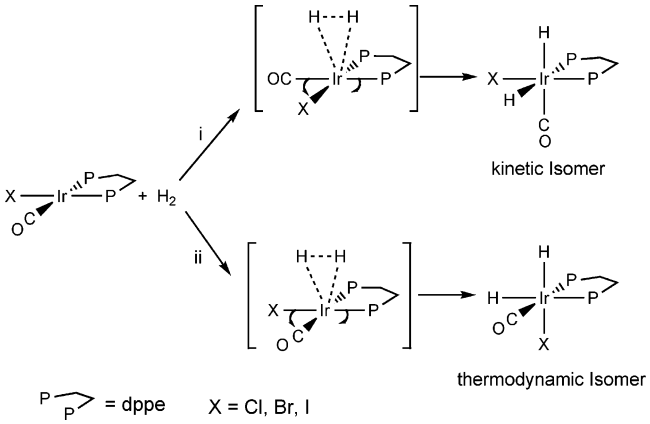

oxidative addition, which occurs early along the reaction coordinate for this exothermic reaction.

Catalytic *asymmetric* hydrogenation is an important class of reactions that has been found to be particularly useful in preparing biologically relevant chiral compounds such as L-dopamine[8] for treatment of Parkinson's disease and aspartame that contains L-phenylalanine as an artificial sweetener.[11] The hydrogenation catalysts used in the preparation of both of these compounds are cationic Rh(I) systems containing chiral bidentate di(phosphine) ligands. The mechanism of asymmetric hydrogenation using Rh(I) catalysts of this type has been studied in detail by Halpern and Landis who found that (a) reversible binding of the prochiral olefin substrate is followed by irreversible reaction with H_2, leading to product and (b) the catalyst−olefin complex present in minor amounts reacts with H_2 much more rapidly than the major diastereomer (by a factor of around 600).[12−17] Hence, from a kinetics standpoint, hydrogen activation is the enantioselective step in the catalysis with ee's for products in excess of 95%.

These studies elegantly illustrate the importance of the detection of minor species in equilibria if an accurate picture of the catalytic pathway is to be assembled. Brown demonstrated by NMR spectroscopy that the less stable enamide isomer reacts substantially faster with H_2 and was responsible for the observed enantiomeric selectivity and, more recently with Bargon, used *p*-H_2 polarization methods to re-examine this process by sensitizing the NMR experiment. They found in this study that an agostic interaction exists in the metal dihydride alkene intermediate.[18]

For model Ir(I) complexes containing chiral di(phosphine) ligands, H_2 oxidative addition would be expected to generate pairs of diastereomers since the cis dihydride product is chiral at the metal center. Several such systems have been examined in this context to see if the diastereoselectivity found for H_2 addition is consistent with the impressive ee's obtained in asymmetric hydrogenations using the cationic Rh catalysts.[19−22] In one study, Kunin et al. employed the chiraphos analogue of the Ir(I) complex shown in Scheme 1 (chiraphos = (2*S*,3*S*)-bis(diphenylphosphino)butane), but found only a 2.1:1 ratio of kinetic diastereomers (those with one hydride trans to P and the other hydride trans to CO) at −25 °C. A more extensive study by Kimmich et al. using $[Ir(COD)(P-P^*)]^+$ complexes found that at −80 °C the ratio of diastereomers formed on oxidative addition was >50:1 for the (*R*)-BINAP ((*R*)-BINAP = (*R*)-2,2′-bis(diphenylphosphino)-1,1′-binaphthyl) derivative and nearly that large for the (*R*,*R*)-Me-DUPHOS analogue ((*R*,*R*)-Me-DUPHOS = (−)-1,2-bis((2*R*,5*R*)-2,5-dimethylphospholano)benzene)). Subsequent conversions to thermodynamic isomers were also followed. In contrast, Yamagata and co-workers observed *no* diastereoselectivity in the reaction of H_2 with $Ir(Cl)(PPh_3)$(*S*-BINAP), obtaining only a 1:1 mixture of diastereomers. Surprisingly, the largest diastereoselectivity for H_2 oxidative addition to an Ir(I) complex was obtained by Shin and Parkin who examined a system containing a pair of chiral *monodentate* phosphole ligands, P*, in a Vaska-type complex of formula *trans*-$IrCl(CO)(P^*)_2$. The observed diastereoselectivity for the meso isomer IrCl(CO)(*R*-P*)(*S*-P*) in which the iridium is a "pseudoasymmetric center" was 60:1, with the reaction proceeding under kinetic control as the initially favored $IrH_2Cl(CO)$(*R*-P*)(*S*-P*) isomer converts to an equilibrium mixture favoring the other isomer.

In this paper, we report the synthesis of two new chiral Ir(I) complexes containing the (*R*)-BINAP ligand and their reactions with H_2. The study of the H_2 oxidative addition chemistry of these complexes is augmented by the use of parahydrogen-induced polarization (PHIP) that can provide greater sensitivity in analyzing reactions of this type.[23−27] PHIP occurs when hydrogen enriched in the para spin state (*p*-H_2) adds pairwise to a compound in such a way that the two ^1H nuclei in the product are magnetically inequivalent. Evidence of PHIP is seen by enhanced absorption and emission lines in product ^1H NMR spectra. PHIP is a dynamic effect, and for it be observed, oxidative addition/reductive elimination of H_2 must occur fast relative to the relaxation of the product hydride protons. The present study

(11) Fuganti, C.; Grasseli, P.; Malpezzi, L. *J. Org. Chem.* **1986**, *51*, 1126−1128.
(12) Landis, C. R.; Feldgus, S. *Angew. Chem. Int. Ed.* **2000**, *39*, 2863−2866.
(13) Landis, C. R.; Brauch, T. W. *Inorg. Chim. Acta* **1998**, *270*, 285−297.
(14) Chan, A. S. C.; Pluth, J. J.; Halpern, J. *J. Am. Chem. Soc.* **1980**, *102*, 5952−5954.
(15) Chua, P. S.; Roberts, N. K.; Bosnish, B.; Okrasinski, S. J.; Halpern, J. *J. Chem. Soc. Chem. Commun.* **1981**, 1278−1280.
(16) Landis, C. R.; Halpern, J. *J. Am. Chem. Soc.* **1987**, *109*, 1746−1754.
(17) Feldgus, S.; Landis, C. R. *Organometallics* **2001**, *20*, 2374−2386.
(18) Giernoth, R.; Heinrich, H.; Adams, N. J.; Deeth, R. J.; Bargon, J.; Brown, J. M. *J. Am. Chem. Soc.* **2000**, *122*, 12381−12382.
(19) Kunin, A. J.; Farid, R.; Johnson, C. E.; Eisenberg, R. *J. Am. Chem. Soc.* **1985**, *107*, 5315−5317.
(20) Kimmich, B. F. M.; Somsook, E.; Landis, C. R. *J. Am. Chem. Soc.* **1998**, *120*, 10115−10125.
(21) Tani, J.; Nakajima, K.; Iseki, A.; Yamagata, T. *Chem. Commun.* **2001**, 1630−1631.
(22) Shin, J. H.; Parkin, G. *J. Am. Chem. Soc.* **2002**, *124*, 7652−7653.
(23) Duckett, S. B.; Sleigh, C. J. *Prog. Nucl. Magn. Reson. Spectrosc.* **1999**, *23*, 71−92.
(24) Eisenberg, R. *Acc. Chem. Res.* **1991**, *24*, 110−116.
(25) Eisenberg, R.; Eisenschmid, T. C.; Chinn, M. S.; Kirss, R. U. *Adv. Chem. Ser.* **1992**, *230*, 47−74.
(26) Natterer, J.; Bargon, J. *Prog. Nucl. Magn. Reson. Spectrosc.* **1997**, *31*, 293−315.
(27) Bowers, C. R. In *Encyclopedia of Nuclear Magnetic Resonance*; Grant, D. M., Harris, R. K., Eds.; John Wiley and Sons: Chichester, 2002; Vol. 9: Advances in NMR, pp 750−770.

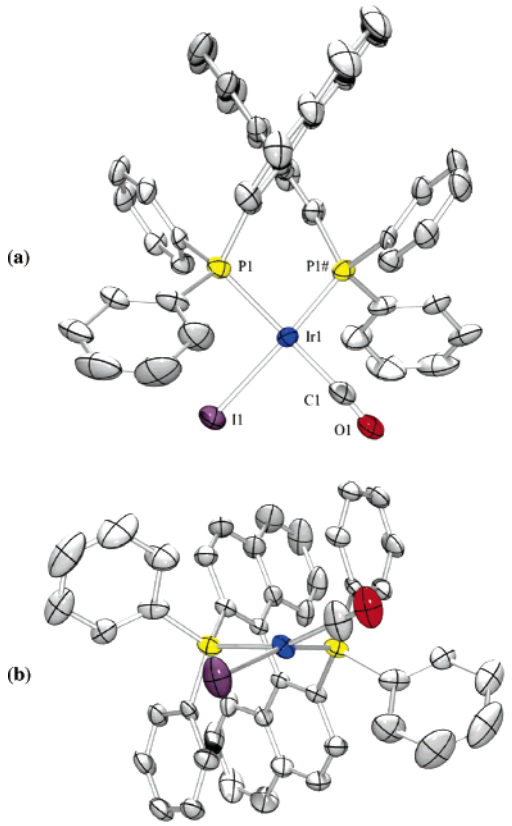

Figure 1. POV-RAY images of **1** showing (a) the labeling of the atoms around the Ir atom and (b) the view through the IrP_2 plane showing its twist relative to the I−Ir−C(O) plane of 25.85(34)°. Displacement ellipsoids are drawn at the 50% level. Hydrogens have been removed for clarity. Selected bond distances (Å) and angles (deg): Ir−P(1), 2.428(1); Ir−P(1#), 2.134(1); Ir−I, 2.643(1); Ir−C(1), 1.861(1); P(1)−Ir−P(1#), 91.79(5); P(1#)−Ir−C(1), 92.0(3); P(1)−Ir−I, 90.32(4); C(1)−Ir−I, 91.1(3); P(1)−Ir−C(1), 160.8(4); P(1#)−Ir−I, 164.08(7).

also analyzes the kinetic and thermodynamic differentiation observed for the possible diastereomeric products.

Results and Discussion

Synthesis and Characterization of IrI(CO)((*R*)-BINAP) (1). Addition of a toluene solution of (*R*)-BINAP to an equimolar solution of $[Bu_4N][IrI_2(CO)_2]$ at room temperature yields a mixture of the mono- and dicarbonyl complexes **1** and $IrI(CO)_2$((*R*)-BINAP), respectively. On filtration of the solution through a pad of alumina, the dicarbonyl species readily eliminates one of its CO ligands to afford the monocarbonyl compound **1** in 74% yield after workup. Recrystallization from toluene and hexanes gives **1** as a dark red powder. The $^{31}P\{^1H\}$ NMR spectrum of **1** is composed of two doublets arising from two inequivalent phosphine atoms at δ 19.12 and 16.65, with J_{PP} of 29.6 Hz. The spectrum is consistent with those obtained for other, previously reported IrX(CO)(P−P) complexes where X = Cl, Br, I and P−P = a chelating diphosphine.[9,19]

Under the ambient temperature reaction conditions described for the synthesis of **1**, the analogous reaction with other chelating di(phosphines) had previously led to formation of the corresponding bis chelate species $[Ir(CO)_x(PP)_2]^+$where $x = 0$, 1 as the major products. The successful formation of IrX(CO)(P−P) analogues of **1** had necessitated that the reaction be initiated at −70 °C under a CO atmosphere and only slowly warmed to room temperature. However, in the case of **1** with BINAP, which forms a 7-membered chelate ring on complexation, no evidence for the bis chelate species was observed, even when BINAP was present in excess as seen by $^{31}P\{^1H\}$ NMR spectroscopy.

Table 1. Crystallographic Data for IrI(CO)((*R*)-BINAP) (**1**) and $[Ir(CO)_2((R)\text{-BINAP})][SbF_6]$ (**2**)

	1	**2**
emp. formula	$C_{45}H_{32}P_2OIIr$	$C_{46}H_{32}P_2O_2SbF_6Ir$
fw	969.75	1106.61
T, K	100.0(1)	100.0(1)
λ, Å	0.71073	0.71073
cryst syst	tetragonal	monoclinic
space group	$P4_12_12$	$P2_1$
Z	4	2
a, Å	12.0023(10)	11.4905(15)
b, Å	12.0023(10)	11.7732(15)
c, Å	26.132(4)	17.234(2)
β, deg	90	102.564(2)
V, Å^3	3764.4(7)	2275.6(5)
ρ_{calcd}, mg/m^3	1.711	1.615
μ, mm^{-1}	4.486	3.644
abs correction	SADABS	SADABS
transm range	0.3523−0.8409	0.3620−0.8388
F(000)	1880	1072
2θ range, deg	1.87−30.99	1.82−29.13°
limiting indices	$-17 \le h \le 17$ $-17 \le k \le 16$ $-37 \le l \le 37$	$-15 \le h \le 15$ $-16 \le k \le 15$ $-23 \le l \le 23$
no. of reflns collected	59810	33354
no. of data/restraints/params	5921/25/250	12078/34/527
GOF	1.010	1.013
R1, wR2 ($I > 2\sigma$)	0.0353, 0.0598	0.0343, 0.0796
R1, wR2 (all data)	0.0729, 0.0689	0.0438, 0.0825

The structure of **1** was confirmed by a single-crystal X-ray diffraction study. Red crystals suitable for X-ray diffraction were grown by slow diffusion of hexanes into a toluene solution of **1**. POV-RAY drawings of the molecular structure of **1** are shown in Figure 1 along with selected bond lengths and angles around the Ir(I) center. A complete tabulation of metrical data for the structure is available in CIF format in the Supporting Information. The molecule lies on a crystallographic 2-fold axis (see Table 1), meaning that disorder must exist in the structure (see the Experimental Section for details of modeling the disorder). The essence of the disorder lies in the carbonyl and iodide positions since these two ligands have steric profiles that are not widely different from a crystallographic standpoint. The BINAP ligand therefore determines the crystal packing arrangement with a 50:50 disorder of iodide and CO, and because of the different bond lengths involving these ligands with the metal center, the iridium atom is also disordered.

While satisfactory final agreement has been reached in refinement of the structure, the disorder model renders the metrical parameters within the coordination sphere of only modest value for comparison purposes. For example, the Ir−P bond length of the phosphine trans to CO (2.428(1) Å), and the Ir−C(O) bond length (1.86(1) Å) are similar to those found in other Ir(I) square planar complexes having CO trans to phosphine (2.328−2.434 Å for Ir−P and 1.804−1.940 Å for Ir−C(O)),[28−31] while the Ir−P bond length of

(28) Cleary, B. P.; Eisenberg, R. *Organometallics* **1992**, *11*, 2335−2337.

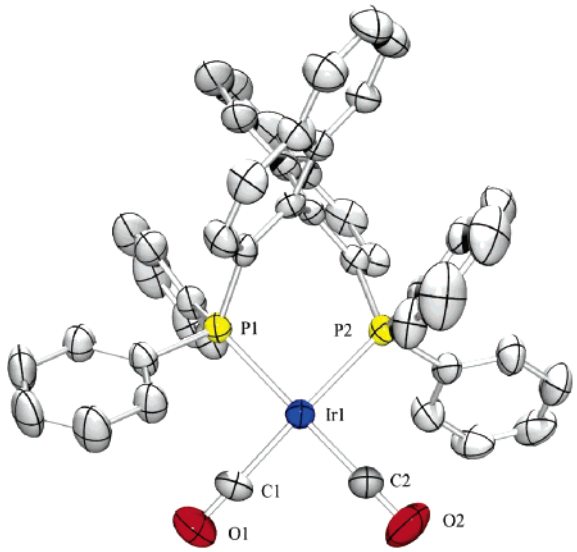

Figure 2. POV-RAY view of **2** showing the labeling of the atoms around the Ir atom. Displacement ellipsoids are drawn at the 50% level. Hydrogens have been removed for clarity. Selected bond distances (Å) and angles (deg): Ir−P(1), 2.357(1); Ir−P(2), 2.364(1); Ir−C(1), 1.916(5); Ir−C(2), 1.870(5); P(1)−Ir−P(2), 92.02(5); P(1)−Ir−C(1), 90.02(18); P(2)−Ir−C(2), 88.7(2); C(1)−Ir−C(2), 90.4(3); P(1)−Ir−C(2), 172.0(2); P(2)−Ir−C(1), 172.0(2).

the phosphine trans to the iodide ligand (2.134(1) Å) is somewhat shorter than that found for similar compounds having phosphine trans to a halide ligand (2.171−2.218 Å).[21,32−34]

A notable feature of the molecular structure of **1** is a significant tetrahedral distortion with a trans P−Ir−C(O) bond angle of 160.8(4)°, a trans P−Ir−I bond angle of 164.08(7)°, and a dihedral angle of 25.85(3)° between the IrP_2 plane and the I−Ir−C(O) plane, as shown in Figure 1.

Synthesis and Characterization of [Ir(CO)$_2$((*R*)-BINAP)][SbF$_6$] (2). Compound **2** is synthesized by the addition of a CH_2Cl_2 solution of $AgSbF_6$ to an equimolar solution of **1** that has been purged with CO. Workup followed by crystallization from CH_2Cl_2 leads to the formation of a pale orange powder of **2** in 97% yield. The $^{31}P\{^1H\}$ NMR spectrum of **2** exhibits only one singlet at δ 12.11, indicating equivalence of the two phosphine donors of the BINAP ligand. The IR spectrum shows two CO stretches at 2084 and 2032 cm^{-1}, consistent with a cationic structure containing two CO ligands occupying cis coordination sites.

The structure of **2** was confirmed by a single-crystal X-ray diffraction study. Dark yellow crystals suitable for X-ray diffraction were grown by slow diffusion of diethyl ether into a methylene chloride solution of **2**. A POV-RAY drawing of the molecular structure of **2** is shown in Figure 2 along with a figure caption that contains selected bond lengths and angles around the Ir(I) center. (A complete tabulation of metrical data is located in the CIF file deposited as Supporting Information.) The crystal structure determination confirms that the geometry around the Ir(I) center is essentially square planar with a minor tetrahedral distortion. Specifically, the two trans P−Ir−C(O) bond angles average 172.0(2)° and the dihedral angle between the planes defined by $Ir(C(O))_2$ and IrP_2 is 11.8°. The Ir−P bond lengths (2.357(1), 2.364(1) Å) and the Ir−C(O) bond lengths (1.916(5), 1.870(5) Å) are similar to those found in other Ir(I) complexes having a CO ligand trans to a P atom (2.328−2.434 Å for Ir−P and 1.804−1.940 Å for Ir−C(O)).[28−31] The difference between the two Ir−C(O) bond lengths, although small, is greater than expected. The reason for this difference is not immediately apparent. One reason inferred from the crystal structure might be the closer proximity of fluorine atom F_1, found in the anion, to the carbon atom in the longer Ir−C bond than to the other carbon atom (2.811(11) vs 2.995(11) Å), although it must be noted that the significance or indeed the presence of such an interaction cannot be determined due to the disorder present in the anion.

Scheme 2

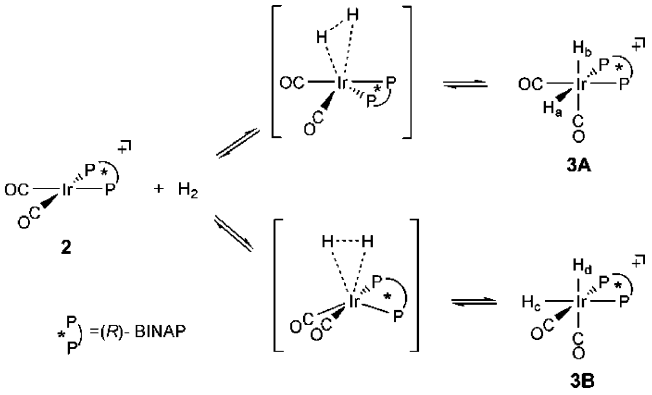

Reaction of [Ir(CO)$_2$((*R*)-BINAP)][SbF$_6$] with H$_2$. The presence of the chiral ligand (*R*)-BINAP in square planar complex **2** means that in concerted H_2 oxidative addition two diastereomers will be produced. For a given enantiomer of the BINAP ligand, the diastereomers differ by virtue of the chirality at the metal center for the *cis,cis*-$[IrH_2(CO)_2$-((*R*)-BINAP)]$^+$product. In light of the C_2 symmetry of complex **2**, the products of H_2 addition from above and below the metal plane are related by symmetry, and hence it is possible to visualize formation of the two diastereomers by simply considering the possible approaches of H_2 to one face of the complex only, as depicted in Scheme 2.

The H_2 oxidative addition reaction was followed by ^1H and $^{31}P\{^1H\}$ NMR spectroscopies. Figure 3 shows the hydride region of ^1H NMR spectra taken 45 s and 2 h after the introduction of H_2 into the reaction solution. The reaction proceeds rapidly, as evidenced by an immediate color change from the light orange of **2** to pale yellow. The initial H_2 addition process proceeds to completion, and once the reaction has commenced, no Ir(I) species can be observed by NMR spectroscopy throughout the remaining course of reaction. The kinetic diastereomer **3A** predominates initially, forming in a ratio to **3B** of >9:1. The ^1H NMR spectrum in

(29) Dahlenburg, L.; Von Deuten, K.; Kopf, J. *J. Organomet. Chem.* **1981**, *216*, 113−127.
(30) Brym, M.; Jones, C.; Waugh, M. *Dalton Trans.* **2003**, 2889−2893.
(31) Schumann, H.; Cielusek, G.; Pickardt, J.; Bruncks, N. *J. Organomet. Chem.* **1979**, *172*, 359−365.
(32) Oster, S. S.; Jones, W. D. *Polyhedron* **2004**, *23*, 2959−2965.
(33) Simons, R. S.; Panzner, M. J.; Tessier, C. A.; Youngs, W. A. *J. Organomet. Chem.* **2003**, *681*, 1−4.
(34) Yamagata, T.; Iseki, A.; Tani, K. *Chem. Letters* **1997**, *12*, 1215−1216.

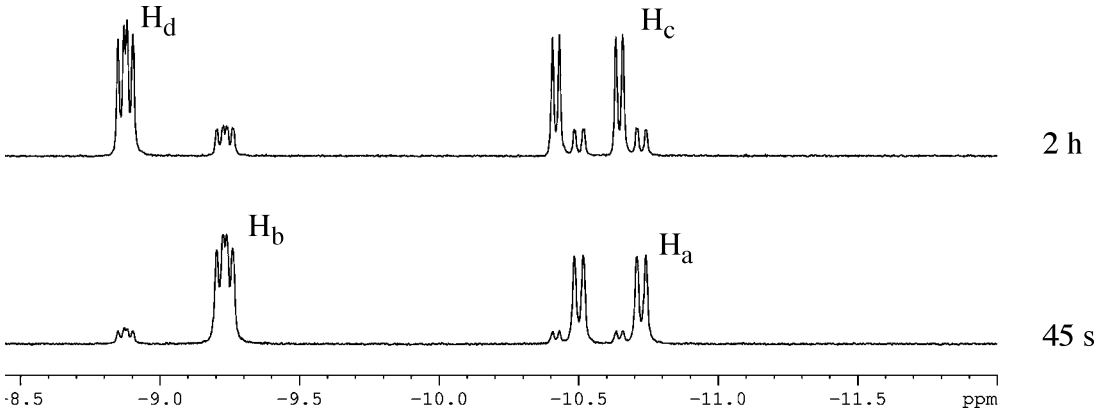

Figure 3. ^{1}H NMR spectra (500 MHz) illustrating the change in the hydride region for the reaction of **2** with H_2 in CD_2Cl_2 as a function of time.

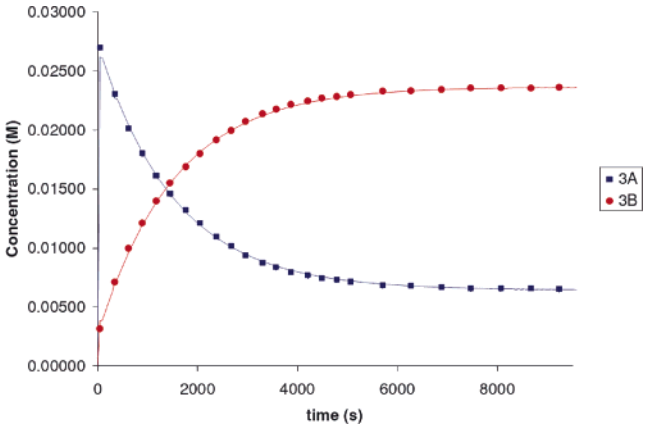

Figure 4. Change in concentration of **3A** (■) and **3B**(●) formed in the reaction of **2** with H_2 as a function of reaction time. The solid line reflects the simulated trace assuming an exponential relaxation to equilibrium.

Figure 3 that was taken after 45 s shows that the two major hydride resonances of **3A** appear as a doublet of doublets at δ −9.2 (H_b) due to almost equivalent couplings to two cis phosphine donors (18 and 19 Hz), and a doublet of doublets (Ha) at δ −10.62 arising from cis and trans phosphorus couplings (16 and 112 Hz, respectively). Over a period of a few hours, the ratio of **3A**/**3B** decreases. The hydride resonances for diastereomer **3B** appear at δ −8.9 (H_d, J_{PH} of 16 and 17 Hz), and −10.6 (H_c, J_{PH} of 12 and 114 Hz) and exhibit similar couplings to those for **3A**, in accordance with the presence of identical coordination geometries. The system relaxes to equilibrium by simple exponential behavior and reaches a final diastereomeric ratio of 1:3.6 (Figure 4).

Extrapolation back to $t = 0$ yields a high initial diastereoselectivity for H_2 oxidative addition of 9.9:1, which corresponds to a $\Delta\Delta G^{\ddagger}_{298}$ of >1.36 kcal/mol for the two different oxidative addition pathways leading to **3A** and **3B**. Moreover, the observed equilibrium ratio of 1:3.6 corresponds to a ΔG_{298} of −0.8 kcal/mol for the **3A** ⇌ **3B** isomerization. The isomerization mechanism for interconverting Ir(III) cis dihydride products from H_2 oxidative addition has previously been considered in terms of a simple reductive elimination/oxidative re-addition sequence and a dihydride transfer path at higher Ir and lower dihydrogen concentrations.[10] Simulations for the reductive elimination/oxidative re-addition isomerization pathway were carried out for the **2** + H_2 system using the KINSIM/FITSIM programs

Table 2. Summary of Simulated Rate Constants for the Reaction of **2** with H_2 at 25 °C[a]

rate constant	k, M^{-1} s^{-1}	rate constant	k, s^{-1}
k_1	0.92 (6)	k_{-1}	6.0 (2) × 10^{-3}
k_2	8.6 (5) × 10^{-2}	k_{-2}	1.53 (1) × 10^{-4}

[a] Simulation parameters: delta time = 50 s; run time = 50 000 s; flux tolerance = 2 × 10^{-2}; iterations/point = 1; integral tolerance = 1 × 10^{-6}. All rate constants were allowed to vary independently. Errors are indicated in parentheses.

to obtain best-fit rate constants for the overall process given in eq 1.[35,36] KINSIM was used to obtain initial fits for concentration data of [**3A**] and [**3B**] versus time (see Supporting Information for detailed data), after which FITSIM was employed to refine the rate constants using a least-squares fit method. The calculated rate constants for the two-step isomerization process are given in Table 2, while the calculated fits of concentration versus time are shown by the solid lines in Figure 4. The fit to the experimental data was excellent with an R^2 value of 1.0000. The calculated rate constants are consistent with the observed diastereoselectivity (k_1/k_2 = 10.7:1) and the equilibrium constant ($K_{eq} = (k_2 \times k_{-1})/(k_1 \times k_{-2}) = 3.67$).

$$\mathbf{3A} \underset{k_{-1}}{\overset{k_1}{\rightleftharpoons}} \mathbf{2} + H_2 \underset{k_{-2}}{\overset{k_2}{\rightleftharpoons}} \mathbf{3B} \qquad (1)$$

Reaction of IrI(CO)((*R*)-BINAP) with H_2 and D_2. The oxidative addition of H_2 to the iodo carbonyl complex **1** leads to the formation of two diastereomeric *pairs* of dihydride products corresponding to the kinetic and thermodynamic isomers shown in Scheme 3. Since complex **1** lacks the C_2 symmetry of dicarbonyl complex **2**, the two faces of the square plane to which H_2 can approach are different and will lead to opposite chirality at the Ir center when H_2 is oriented parallel to a specific axis of the complex. In the diastereomeric pair corresponding to the kinetic isomers (**4A** and **4B**), one hydride ligand is trans to CO and the second is trans to a phosphine donor. In accord with what has been reported previously for other IrX(CO)(P−P) systems, a greater than 95% stereoselectivity is seen for formation of the kinetic diastereomers over the thermodynamic diastereomers.[19] The

(35) Barshop, B. A.; Wrenn, R. F.; Frieden, C. *Anal. Biochem.* **1983**, *130*, 134−135.
(36) Zimmerle, C. T.; Frieden, C. *Biochem. J.* **1989**, *258*, 381−387.

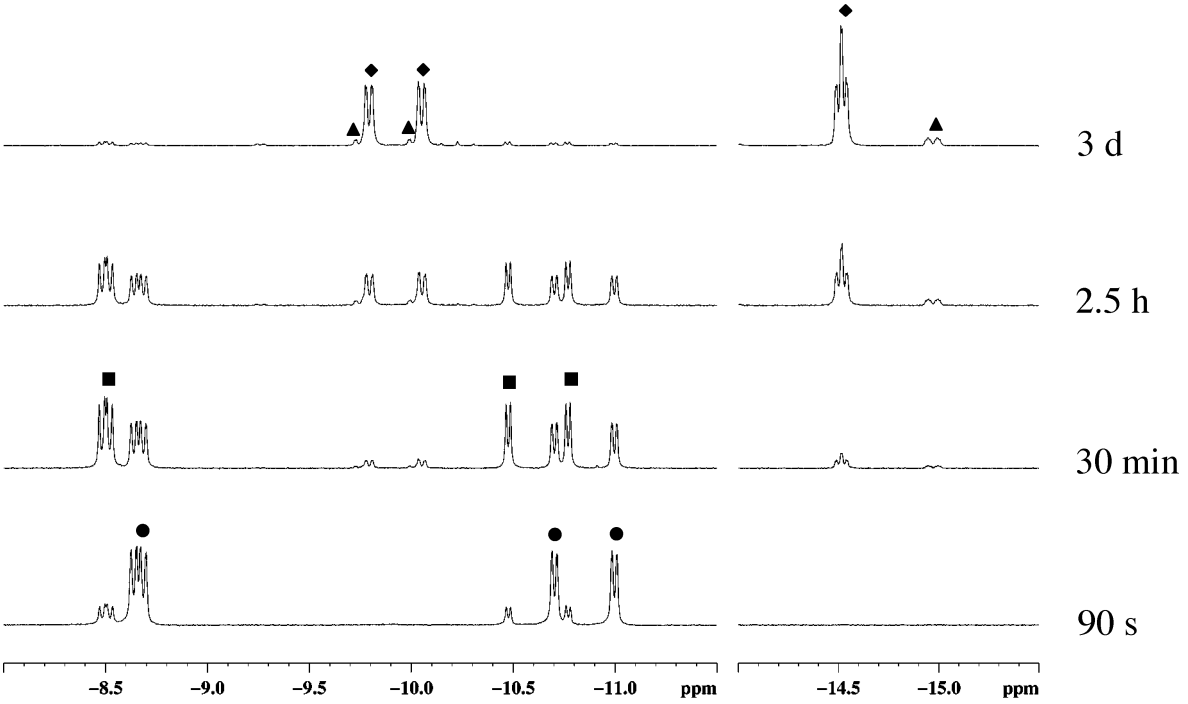

Figure 5. ^{1}H NMR spectra (500 MHz) of the hydride region for the reaction of IrI(CO)((*R*)-BINAP) (**1**) with H_2 in C_6D_6. (●, **4A**; ■, **4B**; ▲, **5A**; ◆, **5B**).

Scheme 3

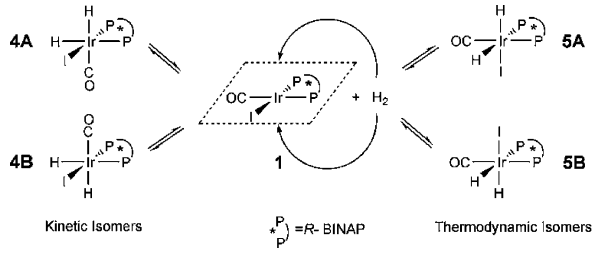

Scheme 4

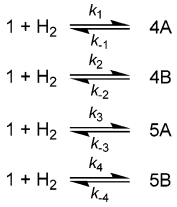

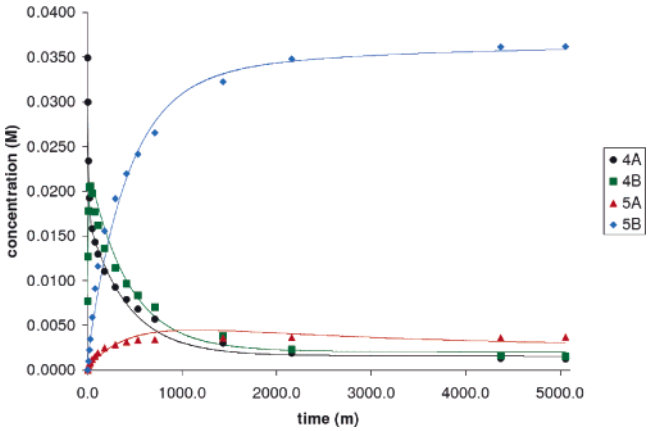

Figure 6. Change in concentration of **4A** (●), **4B** (■), **5A** (▲), and **5B** (◆) formed in the reaction of **1** with H_2 as a function of reaction time. The solid line reflects the simulated trace based on the mechanism in Scheme 4.

reaction is very rapid with an immediate color change from red-orange to pale yellow once H_2 is introduced into the solution. Additionally, as in the oxidative addition of H_2 to **2** to form **3A** and **3B**, a high degree of diastereoselectivity is seen with an initial ratio of **4A**/**4B** of 8.7:1 upon extrapolation to $t = 0$. However, after 20 min, **4B** becomes the predominant species (Figure 5) with an equilibrium ratio of **4A**/**4B** of 1:1.2.

The second pair of diastereomers corresponding to thermodynamic isomers **5A** and **5B** grow in over a period of days. The upfield chemical shift in the hydride resonance that shows cis coupling to both ^{31}P nuclei is indicative of the hydride trans to the iodide ligand.[37] Additionally, within the pair of thermodynamic diastereomers, there exists a significant energetic differentiation, with the more stable isomer being favored by a factor of 10:1. The degrees of kinetic and thermodynamic differentiation seen within each diastereomeric pair of the same $IrH_2I(CO)$((*R*)-BINAP) complex is impressive and shows that even for a molecule as small as H_2, there can exist a significant preference for approach to one of the faces of **1** relative to the other. The results with **1** + H_2 contrast with what was seen with the analogous chiraphos complex that showed a kinetic diastereoselectivity of only 2.1:1 at −25 °C and an equilibrium ratio of the thermodynamic diastereomers of 1.3:1.[19]

Table 3. Summary of Rate Constants Used to Simulate the Reaction of **1** with H_2 at 25 °C

rate constant	k, M^{-1} s^{-1}	rate constant	k, s^{-1}
k_1	0.17	k_{-1}	7.5×10^{-3}
k_2	2.2×10^{-2}	k_{-2}	7.5×10^{-4}
k_3	2.8×10^{-4}	k_{-3}	7.5×10^{-6}
k_4	1.7×10^{-3}	k_{-4}	3.2×10^{-6}

(37) Kaesz, H. D.; Saillant, R. B. *Chem. Rev.* **1972**, *72*, 231−281.

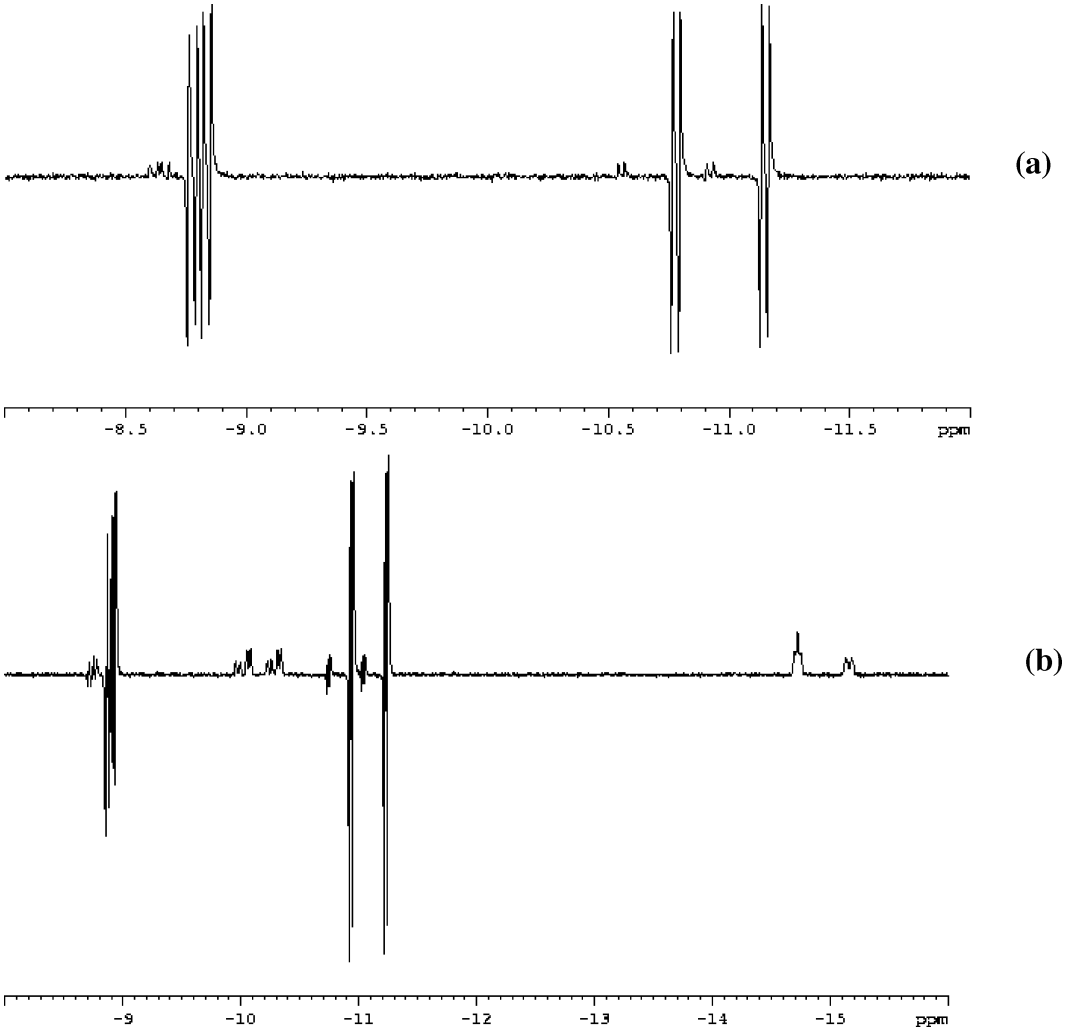

Figure 7. Reaction of the dihydride isomers of **1** with para-enriched hydrogen in C_6D_6 (a) kinetic isomers at room temperature and (b) all four isomers at 85 °C.

Deuterium exchange with the kinetic and the thermodynamic dihydride diastereomers of **1** was also studied. A sample containing mainly the kinetic diastereomers **4A** and **4B** was prepared by shaking an NMR tube containing H_2 and **1** in C_6D_6 for 30 min. At this stage the H_2 in the NMR tube was removed by one freeze−pump−thaw cycle, followed by D_2 addition. Another sample containing mainly the thermodynamic diastereomers **5A** and **5B** was prepared in an analogous fashion by keeping the H_2 in the NMR tube for 4 days before the introduction of D_2 into the sample.

The hydride resonances of **4A** and **4B** rapidly decreased in intensity and completely disappeared at room temperature after 15 min and 3 h, respectively, indicating that, similar to the oxidative addition of H_2 to form the kinetic diastereomers, the reductive elimination of H_2 from them is also rapid. The thermodynamic diastereomers on the other hand did not show any appreciable exchange with D_2 *at room temperature* and required heating at 75 °C for a period of a couple of days for complete exchange with D_2.

As with the **2** + H_2 reaction system, the mechanism of isomerization for **4A**, **4B**, **5A**, and **5B** was probed by simulating the experimental data of the **1** + H_2 reaction using the KINSIM program. Kunin et al. had previously shown that at ambient temperature, the isomerization of the kinetic dihydride isomer of $Ir(H)_2Br(CO)(dppe)$ to its thermodynamic counterpart involved both reductive elimination/oxidative re-addition of H_2 and a bimolecular pathway in which the two hydrides of the kinetic isomer are transferred to a molecule of IrBr(CO)(dppe) to give the thermodynamic isomer while regenerating the Ir(I) species.[10] The latter pathway is dominant when less than 1 equiv of H_2 relative to IrBr(CO)(dppe) exists in the reaction system.

While both pathways were considered in modeling the isomerization of diastereomers **4A**, **4B**, **5A**, and **5B**, only the reductive elimination/oxidative addition sequence was employed in the simulations. The bimolecular path was excluded because ^{31}P NMR measurements of the reaction system revealed the absence of observable amounts of the Ir(I) species **1** needed for the dihydride transfer mechanism and the fact that its inclusion would cause the problem to be underdetermined with up to 16 rate constants. Simulations for the isomerization were therefore based solely on the reductive elimination/oxidative addition mechanism shown in Scheme 4 with eight rate constants.

It was quickly determined, however, that whereas the kinetic diastereomeric ratio could be reasonably determined

by exponential extrapolation to $t = 0$, the rate constant k_1 could not be obtained with any degree of accuracy because the reaction was much more rapid than the observed concentration vs time data (standard deviations of k_1 were always larger than the corresponding rate constants). Therefore, k_1 was given an arbitrary value, large enough to represent the fast initial reaction and small enough to fit the experimental data, and the other rate constants were varied manually to get the best fit to the data. The rate constants for the isomerization process are tabulated in Table 3, while both the experimental and calculated data are shown in Figure 6. These manually adjusted rate constants correspond to an initial kinetic diastereoselectivity (k_1/k_2) of 7.7, and *equilibrium* ratios of 1.3 and 14 for the kinetic (**4B**/**4A** = $(k_2 \times k_{-1})/(k_1 \times k_{-2})$ and thermodynamic isomers (**5B**/**5A** = $(k_4 \times k_{-3})/(k_3 \times k_{-4})$, respectively. They compare favorably with values of 8.7, 1.2, and 10 determined from the actual measurements.

While Scheme 4 is sufficient to model most aspects of the experimental data, it is evident from Figure 6 and the differences between the observed and calculated kinetic diastereoselectivity and thermodynamic isomer equilibrium ratios that other steps, such as the binuclear isomerization pathway, might also be playing a role in the conversion of the kinetic isomers to the thermodynamic isomers.

Reaction of IrI(CO)((*R*)-BINAP) and [Ir(CO)$_2$((*R*)-BINAP)][SbF$_6$] with Parahydrogen. When para-enriched H_2 is added to an NMR tube containing **1** dissolved in C_6D_6, only **4A**, the initially formed kinetic isomer, shows any polarization at room temperature (Figure 7a). Upon heating to 85 °C, **4B** also starts to show polarization (Figure 7b). When parahydrogen is introduced to a solution containing the thermodynamic isomers **5A** and **5B**, no polarization is observed even upon heating to 100 °C.

A similar situation arises when para-enriched dihydrogen is added to a CD_2Cl_2 solution of **2**. Only isomer **3A** shows any polarization, while isomer **3B** shows no polarization even upon heating. Owing to refluxing of the NMR solvent, temperatures above 60 °C were not accessible with this system. These PHIP results for the Ir BINAP complexes **1** and **2** are consistent with the observations of dihydrogen addition discussed above and indicate that with H_2 aligned parallel to a specific axis of the complex, approach from one side of the complex is favored over approach from the other for oxidative addition and the corresponding reductive elimination.

Conclusions

The oxidative additions of dihydrogen to the chiral Ir(I) BINAP complexes **1** and **2** proceed rapidly at room temperature and under kinetic control with a high degree of diastereoselectivity, surpassing those of the previously reported chiraphos analogue. For both **1** and **2**, the kinetically favored dihydride addition products are not the thermodynamically favored isomers, and thermodynamic selectivity is also observed, especially with complex **1**. While the isomerization of **3A** to **3B** can be modeled accurately assuming only a simple reductive elimination/oxidative readdition mechanism, the isomerization of the kinetic isomers **4A** and **4B** to the thermodynamic isomers **5A** and **5B** involve a reductive elimination/oxidative addition *and* possibly other bimolecular dihydride transfer steps. For both complexes **1** and **2**, only the kinetically favored diastereomer shows any polarization when parahydrogen was used.

Experimental Section

General Procedures and Materials. Unless otherwise stated, all reactions and manipulations were performed in dry glassware under a nitrogen atmosphere using either standard Schlenk techniques or an inert-atmosphere glovebox. CH_2Cl_2, hexanes, and diethyl ether were purified as described by Grubbs.[38] Dichloromethane-d_2 and benzene-d_6 were purchased from Cambridge Isotope in ampules and used without further purification. (*R*)-BINAP and $AgSbF_6$ were purchased from Aldrich and used without any further purification. Parahydrogen was prepared by cooling high-purity hydrogen over $FeCl_3$ adsorbed onto silica at 77 K.[39] All NMR spectra were recorded on a Bruker Avance 500 MHz spectrometer. ^{1}H chemical shifts (δ in ppm) are referenced using chemical shifts of residual solvent resonances. ^{31}P chemical shifts (δ in ppm) are relative to an external 85% solution of phosphoric acid in the appropriate solvent. Mass spectrometric data were obtained on a Hewlett-Packard Series 1100 MSD fitted with an atmospheric pressure ionization chamber. Elemental analyses were performed by Desert Analytics, Inc.

IrI(CO)((*R*)-BINAP) (1). A 10 mL toluene solution of (*R*)-BINAP (0.410 g, 1.32 mmol) was added to a 20 mL toluene solution of [TBA][IrI$_2$(CO)$_2$] (0.490 g, 1.32 mmol). After the mixture was stirred for 15 min, the color of the solution turned to dark orange and [TBA]I precipitated. After filtration through a pad of alumina, a dark red colored solution is obtained. Upon addition of hexanes, **1** is obtained as a reddish powder in a 74% yield. ^{1}H NMR (C_6D_6, ppm): δ 8.35−6.41 (overlapping naphthyl and aryl H); ^{31}P{^{1}H} NMR (C_6D_6, ppm): δ 19.12 (d, J_{PP} = 29.6 Hz, 1 P), 16.65 (d, J_{PP} = 29.6 Hz, 1 P). Anal. Calcd for $C_{45}H_{32}P_2OIIr$: C, 55.73; H, 3.33. Found C, 55.67; H, 3.26.

[Ir(CO)$_2$((*R*)-BINAP)][SbF$_6$] (2). CO is bubbled through a 10 mL CH_2Cl_2 solution of **1** (0.337 g, 0.347 mmol). The color of the solution turns to light orange after which a 5 mL CH_2Cl_2 solution of $AgSbF_6$ (0.120 g, 0.347 mmol) is added. AgI is removed by filtration, and complex **2** is precipitated as a pale orange powder by the addition of diethyl ether, in a 97% yield. IR (KBr, cm^{-1}) 2084 (s, CO), 2032 (s, CO); ^{1}H NMR (CD_2Cl_2, ppm): δ 7.92−7.83 (m, 4 H), 7.77−7.67 (m, 10 H), 7.45 (t, 7.3 Hz, 2 H), 7.49−7.42 (m, 2 H), 7.42−7.32 (m, 4 H), 7.3 (t, 7.5 Hz, 2 H), 7.04 (t, 7.2 Hz, 2 H), 6.91−6.82 (m, 4 H), 6.71 (d, 8.5 Hz, 2 H); ^{31}P{^{1}H} NMR (CD_2Cl_2, ppm): δ 12.11 (s); MS (*e*/*z*) 871.3 ([Ir(CO)$_2$((*R*)-BINAP)]$^+$). Anal. Calcd for $C_{46}H_{32}P_2O_2SbF_6Ir$: C, 49.92; H, 2.91. Found C, 50.16; H, 2.76.

General Procedure for the Reaction of 1 or 2 with H_2 or Para-Enriched Hydrogen. A resealable NMR tube was charged with **1** (0.005 g) and 0.6 mL of C_6D_6 (CD_2Cl_2 for **2**). After the solution was subjected to two freeze−pump−thaw cycles, the NMR tube was back-filled with H_2. The valve was closed, the solution was allowed to thaw, and the NMR tube was then shaken vigorously to promote solution−gas mixing. The reaction was then monitored periodically by ^{1}H and ^{31}P NMR spectroscopies.

(38) Pangborn, A. B.; Giardello, M. A.; Grubbs, R. H.; Rosen, R. K.; Timmers, F. J. *Organometallics* **1996**, *15*, 1518−1520.
(39) Millar, S. P.; Jang, M.; Lachicotte, R. J.; Eisenberg, R. *Inorg. Chim. Acta* **1998**, *270*, 363−375.

3A. ^{1}H NMR (CD_2Cl_2, ppm): δ 8.20−6.65 (naphthyl and aryl H's overlapping with those of **3B**), −9.23 (dd, J_{PP} = 18.3 Hz, 10.2 Hz, 1 H), −10.62 (dd, J_{PP} = 113.1 Hz, 14.9 Hz, 1H); ^{31}P{^{1}H} NMR (CD_2Cl_2, ppm): δ 0.09 (d, J_{PP} = 15.2 Hz, 1 P), −2.70 (d, J_{PP} = 17.6 Hz, 1 P).

3B. ^{1}H NMR (CD_2Cl_2, ppm): δ 8.20−6.65 (naphthyl and aryl H's overlapping with those of **3A**), −8.89 (dd, J_{PP} = 15.9 Hz, 11.1 Hz, 1 H), −10.50 (dd, J_{PP} = 113.1 Hz, 13.2 Hz, 1 H); ^{31}P{^{1}H} NMR (CD_2Cl_2, ppm): δ 10.6 (d, J_{PP} = 18.4 Hz, 1 P), −2.70 (d, J_{PP} = 15.3 Hz, 1 P).

4A. ^{1}H NMR (C_6D_6, ppm): δ 8.55−6.30 (naphthyl and aryl H's overlapping with those of **4B, 5A**, and **5B**), δ −8.67 (dd, J_{PP} = 23.9 Hz, 14.2 Hz, 1 H), −10.83 (dd, J_{PP} = 149.6 Hz, 12.3 Hz, 1 H); ^{31}P{^{1}H} NMR (C_6D_6, ppm): δ −6.95 (d, J_{PP} = 7.4 Hz, 1 P), −3.91 (d, J_{PP} = 7.4 Hz, 1 P).

4B. ^{1}H NMR (C_6D_6, ppm): δ 8.55−6.30 (naphthyl and aryl H's overlapping with those of **4A, 5A**, and **5B**), δ −8.51 (dd, J_{PP} = 18.2 Hz, 14.1 Hz, 1 H), −10.61 (dd, J_{PP} = 150.1 Hz, 11.2 Hz, 1 H); ^{31}P{^{1}H} NMR (C_6D_6, ppm): δ 16.22 (d, J_{PP} = 7.4 Hz, 1 P), −3.51 (d, J_{PP} = 7.4 Hz, 1 P).

5A. ^{1}H NMR (C_6D_6, ppm): δ 8.55−6.30 (naphthyl and aryl H's overlapping with those of **4A, 4B**, and **5B**), δ −9.88 (ddd, J_{PP} = 137.5 Hz, 18.5 Hz, J_{HH} = 4.8 Hz 1 H), −14.96 (ddd, J_{PP} = 23.6 Hz, 12.1 Hz, J_{HH} = 4.6 Hz 1 H); ^{31}P{^{1}H} NMR (C_6D_6, ppm): δ −2.45 (d, J_{PP} = 18.75 Hz, 1 P), −5.65 (d, J_{PP} = 18.75 Hz, 1 P).

5B. ^{1}H NMR (C_6D_6, ppm): δ 8.55−6.30 (naphthyl and aryl H's overlapping with those of **4A, 4B**, and **5A**), δ −9.92 (ddd, J_{PP} = 130.5 Hz, 14.6 Hz, J_{HH} = 3.9 Hz 1 H), −14.51 (td, J_{PP} = 13.3 Hz, J_{HH} = 3.7 Hz 1 H); ^{31}P{^{1}H} NMR (C_6D_6, ppm): δ 11.72 (d, J_{PP} = 18.64 Hz, 1 P), −15.49 (d, J_{PP} = 18.84 Hz, 1 P).

Crystal Structure Determinations. For each structure determination, a crystal was placed onto the tip of a 0.1 mm diameter glass fiber and mounted on a Bruker SMART APEX II Platform CCD diffractometer (Mo Kα radiation, graphite monochromator) for data collection at 100.0(1) K. A preliminary set of cell constants and an orientation matrix were calculated from 158 (**1**) and 472 (**2**) reflections harvested from three sets of 20 frames, oriented such that orthogonal wedges of reciprocal space were surveyed: four major sections of frames were collected with 0.50° (**1**) or 0.30° (**2**) steps in ω at four different ϕ settings and a detector position of −28° in 2θ. The intensity data were corrected for absorption.[40] The data collection for each determination was carried out using Mo Kα radiation (graphite monochromator). Final cell constants were calculated from the *xyz* centroids of 3536 strong reflections from the actual data collection after integration.

Each structure was solved using SHELXS-97[41] and refined using SHELXL-97.[41] Space groups $P4_12_12$ (**1**) and $P2_1$(**2**) were determined on the basis of systematic absences and intensity statistics. For each determination, a direct-methods solution was calculated which provided most non-hydrogen atoms from the E-map. Full-matrix least-squares/difference Fourier cycles were performed which located the remaining non-hydrogen atoms. All non-hydrogen atoms were refined with anisotropic displacement parameters. All hydrogen atoms were found from the difference map and refined with relative isotropic displacement parameters. A summary of experimental and refinement details can be found in Table 1.

Details for the Structure of 1. The molecule lies on a crystallographic 2-fold axis; thus, one-half of the molecule is unique. The iridium atom and the iodide and carbonyl ligands are disordered over the 2-fold axis (50:50). Additionally, one of the phenyl rings is modeled as disordered over two positions (50:50, because it is coupled to the I/CO disorder).

Details for the Structure of 2. The cation and anion are well separated, and all atoms lie on general positions. The anion is modeled as disordered over two positions (58:42).

Acknowledgment. We gratefully acknowledge Prof. W. D. Jones, Prof. H. A. Stern, and T. A. Atesin for assistance with the kinetic simulations and Dr. D. J. Fox for helpful discussions. We also thank the National Science Foundation (Grant No. CHE-0092446) and the donors of the Petroleum Research Fund for support of this work.

Supporting Information Available: Plots of the extrapolation of experimental data and tabulated experimental vs calculated data for the reactions of **2** + H_2 and **1** + H_2, crystal data, atomic coordinates, bond distances, bond angles, and anisotropic displacement parameters for **1** and **2** in CIF format. This material is available free of charge via the Internet at http://pubs.acs.org.

IC061471A

(40) The SADABS absorption correction program is based on the method of Blessing; see Blessing, R. H. *Acta Crystallogr. Sect A* **1995**, *51*, 33−38.

(41) *SHELXTL: Structure Analysis Program, version 5.04*; Siemens Industrial Automation, Inc.: Madison, WI, 1995.